International Journal of Numerical Methods for Heat & Fluid Flow

Effect of tilt angle on the multi-pipe channel with sinusoidal/curved walls - numerical modelling based on finite volume method

Payam Hooshmand, Mohammad Bahrami, Navid Bagheri, Meysam Jamshidian, Emad Hasani Malekshah,

Effect of tilt angle on the multi-pipe channel with sinusoidal/curved walls – numerical modelling based on finite volume method

Received 19 July 2018
Revised 10 October 2018
Accepted 24 October 2018

Payam Hooshmand
Department of Mechanical Engineering, Sanandaj Branch, Islamic Azad University, Sanandaj, Iran

Mohammad Bahrami and Navid Bagheri
Young Researchers and Elites Club, Science and Research Branch, Islamic Azad University, Tehran, Iran

Meysam Jamshidian
Department of Natural resources and Environment, Science and Research Branch, Islamic Azad University, Tehran, Iran, and

Emad Hasani Malekshah
Faculty of Engineering Computer and Mathematical Sciences, University of Adelaide, Adelaide, Australia

Abstract

Purpose – This paper aims to investigate the two-dimensional numerical modeling of fluid flow and heat transfer in a fluid channel.

Design/methodology/approach – The channel is filled with the CuO-water nanofluid. The KKL model is used to estimate the dynamic viscosity and considering Brownian motion. On the other hand, the influence of CuO nanoparticles' shapes on the heat transfer rate is taken account in the simulations. The channel is included with several active pipes with hot and cold temperatures. Furthermore, the external curved and sinusoidal walls have cold and hot temperatures, respectively.

Findings – Three different tilt angles are considered with similar boundary and operating conditions. The Rayleigh numbers, solid volume fraction of CuO nanoparticles in the pure water and the tilt angles are the governing parameters. Different cases studies, such as streamlines, heat transfer rate, local and total entropy generation and heatlines, are analysed under influences of these governing parameters.

Originality/value – The originality of this work is investigation of fluid flow, heat transfer and entropy generation within a nanofluid filled channel using FVM.

Keywords CuO-water nanofluid, KKL model, Finite volume method, Multi-pipe channel, Tilt angle

Paper type Research paper

Nomenclature

CS = control surface;
CV = control volume;
dA = infinitesimal surface area;

International Journal of Numerical Methods for Heat & Fluid Flow
© Emerald Publishing Limited
0961-5539
DOI 10.1108/HFF-07-2018-0390

dS = infinitesimal surface;
dV = infinitesimal volume;
$\dot{S}_l$ = Local entropy generation;
$\dot{S}_{l,\ f}$ = fluid friction irreversibility;
$\dot{S}_{l,\ h}$ = heat transfer irreversibility;
$\dot{S}_T$ = Total entropy generation;
gy = acceleration of gravity;
Gr = Grashof number ($Gr = g\beta\Delta TL^3/v^2$);
Ge = Gebhart number ($Ge = g\beta H/CP$);
k = thermal conductivity [$W/m \cdot k$];
Be = Bejan number;
L = Length of wall;
R = Radius of cavity;
r_1 = Diameter of freezing core;
r_2 = Diameter of active body;
Nu_{Avg} = average Nusselt number;
Nu_{Local} = Local Nusselt number;
Pr = Prandtl number;
T = fluid temperature;
u, v = velocity components; and
x, y = Cartesian coordinates.

Greek symbols
α = thermal diffusivity;
ϕ = solid volume fraction;
φ = dimensionless viscous dissipation;
θ = dimensionless temperature ($\theta = (T - T_C)/(T_H - T_C)$);
ν = kinematic viscosity;
ρ = fluid density;
ψ = stream function; and
β = thermal expansion coefficient.

Subscripts
nf = nanofluid;
f = base fluid; and
P = Solid particle.

1. Introduction

The natural convection fluid flow and heat transfer have many applications in different industrial and engineering projects. Some of these applications can be mentioned as geothermal systems, double-pane window, furnaces, etc. Because of this matter, many investigations have been carried out to analyse different effective parameters on the natural convection phenomenon (Ben-Nakhi and Chamkha, 2007a, 2007b, 2006a, 2006b).

There are lots of literatures which apply the numerical methods to investigate the fluid flow and heat transfer of natural convection using different numerical methods, operating fluids, boundary conditions and so on (Purusothaman *et al.*, 2016a, 2016b, 2016c, 2016d; Purusothaman, 2018). The work which was done by Patankar (1980) apply inverse methods to investigate the behaviour of natural convection which is very powerful and simple method. There are other works which apply the numerical method such as

Verhoeven (1969), Lewis *et al.* (1996) and Ferziger and Peric (2012). Bianchi *et al.* (2004) investigate the natural convection within a closed cavity. Bejan (2013) obtained an outstanding work which provides tools for systems sizing. It is obvious that the real prototype must be modelled accurately to simulate the real conditions of phenomena as close as possible. To cite this kind of studies, Suárez *et al.* (2012) numerically studied a real application in the field of building to compare the energy performance of a conventional horizontal open joint ventilated façade with a typical one. All of the researchers search to find the methods to obtain the results with high reliability. It is clear that most of the phenomena must be modelled in three-dimensional (3D) form to obtain a comprehensive view. To achieve this goal, some works studied the 3D natural convection. Recently, Salari *et al.* (2017a) carried out a 3D numerical simulation of natural convection and entropy generation with an enclosure filled by two immiscible fluids of MWCNTs and air to simulate the real condition of many phenomena with two fluids such as a cell of Lead-Acid battery. Koca *et al.* (2007) studied the natural convection within a triangular enclosure filled with air ($Pr = 0.71$) with localized heat source at the bottom of the enclosure and consider the effects of Prandtl number. At low Rayleigh number $10^3 < Ra < 10^4$, it was observed that the fluid rises from the middle of the enclosure and falls down from the sides. This kind of fluid flow caused to form two main circulation cells. Because of inclined wall at right section of the enclosure, fluid movements were weaker at this section, so the size of eddies became smaller at this part.

In the present investigation, the hydrothermal aspects of natural convection phenomenon in a fluid channel with active pipes are analysed. The entropy generation and heatline visualization are used to fortify the analysis. On the other hand, the average Nusselt number, total magnitude of entropy generation and Bejan number are presented.

2. Problem definition and boundary simplifications

In the present work, the natural convection and entropy generation within a channel with active pipes under influence of different governing parameters, such as Rayleigh number, nanoparticle concentration and tilt angles, are investigated. There is a nanofluid channel, which is as like a quarter of circle, included with different injection pipes. To present the problem properly, the 3D schematic of fluid channel is presented in Figure 1. It is note that the physical and thermal boundary conditions are same along *z*-axis which makes the

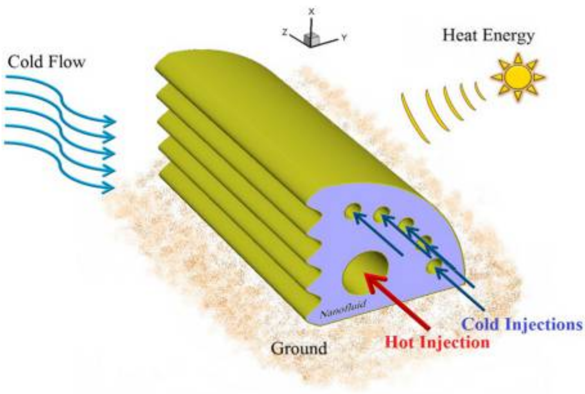

Figure 1.
3D presentation of problem

two-dimensional (2D_ simulation possible. The heat energy, which can be issued by a heat source like sun, is applied to curved wall. On the other hand, the cold stream, which can be issued by wind flow, is applied to sinusoidal wall. In addition, the bottom of the channel is covered by the ground. In the present problem, different simplifications are preformed to simplify the boundary conditions as below:

- Heat energy to curved wall is considered as constant hot curved wall.
- Cold flow to sinusoidal wall is considered as constant cold sinusoidal wall.
- Bottom wall covered by ground is considered as adiabatic wall.
- Internal injection pipes are considered as internal active bodies with constant temperature.

These simplifications on the thermal boundary conditions are presented in a 2D section.

The 2D physical and thermal boundary conditions are represented in Figure 2. The lengths of horizontal and vertical external walls are equal and presented by L. Moreover, the radius of circle is presented by R which is equal to L. The radius of hot and cold pipes are shown by $r_1 = \frac{3}{10}R$ and $r_2 = \frac{1}{10}R$, respectively.

Three different tilt angles are selected to be investigated, as shown in Figure 3. As it can be observed in Figure 3, three tilt angles with $\theta = 0°$, 45° and 90° with similar physical and thermal boundary conditions are selected.

3. Governing equations and numerical approach

3.1 Governing equations

The steady-state laminar flow regime is selected as these conditions are usually occurs in the engineering equipment where the natural convection is the main heat transfer mechanism. The operating fluid, which is a type of nanofluid, is modelled as a Newtonian fluid as the effect of

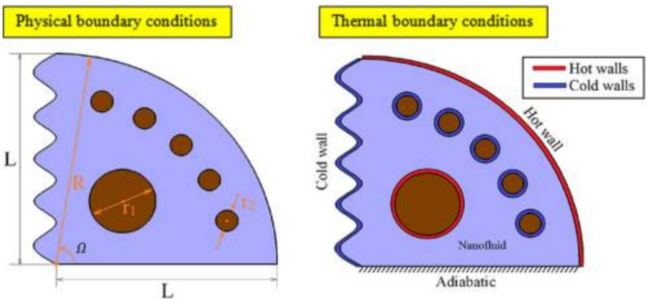

Figure 2.
Presentation of physical and thermal boundary conditions

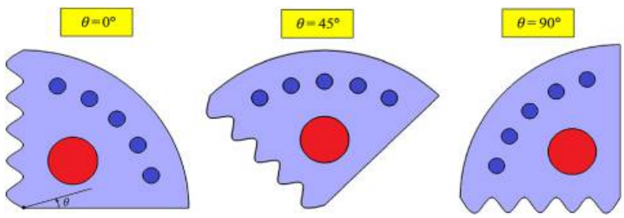

Figure 3.
Presentation of tilt angles

temperature on the nanofluid is neglected. On the other hand, the Boussinesq approximation is used to account the buoyancy force in the simulations. As a matter of fact, this approximation states that the density variation is only important in the combined term buoyancy-weight and it is expressed by the volumetric expansion coefficient as equation (1):

$$\beta = -\frac{1}{\rho}\left(\frac{\partial \rho}{\partial T}\right)_P \tag{1}$$

The governing equations for mass, momentum and energy balance are represented respectively as below (Malekshah *et al.*, 2018; Salari *et al.*, 2017b, 2018a, 2018b):

$$\frac{\partial u_i}{\partial x_i} = 0, \tag{2}$$

$$\frac{\partial u_i u_j}{\partial x_j} = -\frac{1}{\rho}\frac{\partial p}{\partial x_i} + g_i \beta (T - T_L) + \nu \left(\frac{\partial^2 u_i}{\partial x_j^2}\right) \tag{3}$$

$$\frac{u_j T}{\partial x_j} = \alpha \left(\frac{\partial^2 T}{\partial x_j^2}\right) \tag{4}$$

The problem variables are changed to dimensionless forms for the better analysis as below:

- $U_i = \frac{u_i L}{\nu}$,
- $X_i = \frac{x_i}{L}$,
- $\theta = \frac{T - T_L}{T_H - T_L} = \frac{T - T_L}{\Delta T}$,
- $P = \frac{pL^2}{\nu^2 \rho}$.

Where u_i, x_i represent the i-components of velocity and position, respectively. L is the characteristic length, ν is the kinematic viscosity, T is the temperature, p is the pressure, and T_L and T_H state the cold and hot temperatures, respectively.

3.2 Thermo-physical properties of nanofluid

The thermo-physical properties of nanofluid should be modified. The specific heat energy $(\rho C_P)_{nf}$, thermal expansion coefficient $(\rho\beta)_{nf}$ and electrical conductivity σ_{nf} of nanofluid are defined as follows (Rahimi *et al.*, 2018f):

$$(\rho C_P)_{nf} = (\rho C_P)_f (1 - \varphi) + (\rho C_P)_s \varphi, \tag{5}$$

$$\rho_{nf} = \rho_f (1 - \varphi) + \rho_s \varphi, \tag{6}$$

$$(\rho\beta)_{nf} = (\rho\beta)_f (1 - \varphi) + (\rho\beta)_s \varphi, \tag{7}$$

The dynamic viscosity of nanofluid (μ_{nf}) can be calculated using KKL model (Rahimi *et al.*, 2018c):

$$\mu_{eff} = \mu_{static} + \mu_{Brownian} = \mu_{static} + \frac{k_{Brownian}}{k_f} \times \frac{\mu_f}{Pr_f}$$

$$k_{Brownian} = 5 \times 10^4 g'(\varphi,\ T,\ d_P)\varphi\rho_f C_{Pf}\sqrt{\frac{\kappa_b T}{d_P \rho_P}}$$

$$g'(\varphi,\ T,\ d_P) = Ln(T)\left(a_1 + a_2 Ln(d_P) + a_3 Ln(\varphi) + a_4 Ln(d_P)Ln(\varphi) + a_5 Ln(d_P)^2\right) + \left(a_6 + a_7 Ln(d_P) + a_8 Ln(\varphi) + a_9 Ln(\varphi)Ln(d_P) + a_{10} Ln(d_P)^2\right) \quad (8)$$

The thermo-physical properties of CuO-water nanofluid are provided in Table I.

The coefficient values of CuO-water nanofluid are obtained in Table II.

The thermal conductivity of nanofluid (k_{nf}) is defined as follows (Kandelousi, 2014):

$$\frac{k_{nf}}{k_f} = \frac{-m(k_f - k_P)\varphi + (k_P - k_f)\varphi + mk_f + k_P + k_f}{mk_f + (k_f - k_P)\varphi + k_f + k_P} \quad (9)$$

where m is the shape factor. Different magnitudes of shape factors for different nanoparticles' shapes are obtained in Figure 4.

3.3 Non-dimensional forms of governing equations

Using defined dimensionless parameters in the previous section, the mass, momentum and energy equations are changed to dimensionless form. The non-dimensional balance equations are presented in integral form as below (Fontes *et al.*, 2017):

Table I. The thermo-physical properties of CuO-water nanofluid

Material	$\rho(kg/m^3)$	$C_P(j/Kg \cdot K)$	$k(W/m \cdot K)$	$d_P(nm)$	$\sigma(\Omega \cdot m)^{-1}$
Pure water	997.1	4,179	0.613	–	0.05
CuO nanoparticles	6,500	540	18	29	2.7×10^{-8}

Table II. The coefficient values of CuO-water nanofluid

Coefficient values	CuO-water
a_1	−26.593310846
a_2	−0.403818333
a_3	−33.3516805
a_4	−1.915525591
a_5	6.421858E-02
a_6	48.40336955
a_7	−9.787756683
a_8	190.245610009
a_9	10.9285386565
a_{10}	−0.72009983664

$$\int_{CS} U_j \cdot n_j dS = 0, \tag{10}$$

$$\int_{CS} U_i U_j \cdot n_j dS = -\int_{CS} P\delta_{ij} \cdot n_j dS - \int_{CV} Gr\theta dV + \int_{CS} \left[\left(\frac{\partial U_i}{\partial X_j} + \frac{\partial U_j}{\partial X_i}\right)\right] \cdot n_j dS, \tag{11}$$

$$\int_{CS} \theta U_j \cdot n_j dS = \int_{CS} Pr^{-1} \frac{\partial \theta}{\partial X_j} \cdot n_j dS, \tag{12}$$

where Gr is the Grashof number, which is defined as $Gr = \frac{g\beta\Delta TL^3}{\nu^2}$, declaring the relationship and ratio between buoyancy and viscous forces. Furthermore, Pr is the Prandtl number, which is defined as $Pr = \frac{\nu}{\alpha}$, declaring the ratio of kinematic to thermal diffusivities.

The Finite Volume Method (FVM) is used to discretize the governing equations during the simulations. The SIMPLE algorithm has been used. To discrete the convection terms, the second-order upwind approach is used. Also, the central differencing scheme is used to discrete the diffusive terms.

3.4 Entropy generation formulation

The total generated entropy $\left(S'_g\right)$ during the natural convection within the computational domain is defined as follows (Rahimi *et al.*, 2018e, 2018b):

$$S'_g = \left\{\frac{k_{nf}}{T_0{}^2}\left[\left(\frac{\partial T'}{\partial x}\right)^2 + \left(\frac{\partial T'}{\partial y}\right)^2\right]\right\} + \frac{\mu_{nf}}{T_0}\left\{2\left[\left(\frac{\partial V'_x}{\partial x}\right)^2 + \left(\frac{\partial V'_x}{\partial y}\right)^2\right] + \left(\frac{\partial V'_y}{\partial x} + \frac{\partial V'_x}{\partial y}\right)^2\right\} \tag{13}$$

The dimensionless form of total entropy generation (N_S) is deified as follows (Rahimi *et al.*, 2018a):

Shape factor (m)	Spherical		3
	Platelet		5.7
	Cylinder		4.8
	Brick	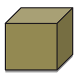	3.7

Figure 4.
The magnitudes of shape factor of different nanoparticles' shapes

$$N_s = \left(\frac{k_{nf}}{k_f}\left[\left(\frac{\partial T}{\partial X}\right)^2 + \left(\frac{\partial T}{\partial Y}\right)^2\right]\right) + \left(\varphi_s \frac{\mu_{nf}}{\mu_f}\left\{2\left[\left(\frac{\partial V_x}{\partial X}\right)^2 + \left(\frac{\partial V_y}{\partial Y}\right)^2\right] + \left[\left(\frac{\partial V_y}{\partial X} + \frac{\partial V_x}{\partial Y}\right)^2\right]\right\}\right) \tag{14}$$

where $\varphi_s = \left(\frac{\alpha}{l\Delta T}\right)^2 T_0$ is defined as the irreversibility coefficient.

The dimensionless total entropy generation can be calculated by integrating the local dimensionless generated entropy in the computational domain as follows:

$$S_{total} = \int N_s dv \tag{15}$$

The average Nusselt number over the desired walls is defined as follows (Rahimi *et al.*, 2018d; Mahmoud *et al.*, 2017):

$$Nu = \frac{k_{nf}}{k_f}\frac{\partial T}{\partial r} \quad and \quad Nu_{avg} = \int_0^{90} Nu \; d\Omega \tag{16}$$

4. Validation and grid independency analysis

Three different works are selected to validate the present numerical simulations. For the first one, the magnitudes of mean Nusselt number based on different Rayleigh number and solid volume fraction of Cu nanoparticles are compared with those obtained results presented by Oztop and Abu-Nada (2008) and Sheikhzadeh *et al.* (2011), shown in Figure 5. The mean Nusselt number is calculated during natural convection in a partially-heated square cavity filled with Cu-water nanofluid. It can be seen that there are close agreements between the results at all Rayleigh numbers and nanoparticle concentrations. For further validation, the obtained Bejan number are compared with those obtained result presented by Oliveski *et al.* (2009) and Khorasanizadeh *et al.* (2013), as shown in Table III, at two different Rayleigh numbers and irreversibility distribution ratios (Φ).

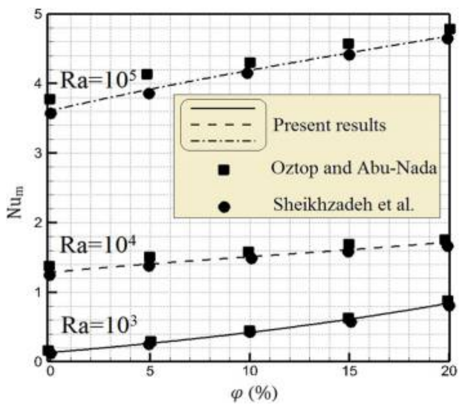

Figure 5.
Comparison of mean Nusselt number with the published results of Oztop and Abu-Nada (2008) and Sheikhzadeh *et al.* (2011)

To show the independency of the present results with respect to the mesh distributions, the grid independency analysis is performed. The averaged Nusselt number at the surface of curved wall at two different Rayleigh numbers and tilt angles are presented at six mesh distributions in Table IV. It can be concluded that the 91 × 271 is fairly appropriate mesh distributions for further simulations.

5. Results and discussion

The natural convection and entropy generation in a fluid channel are analysed, comprehensively. The streamlines, temperature filed, local fluid friction and heat transfer irreversibility maps and heatlines under influence of Rayleigh number, nanoparticle concentration and tilt angle are presented, graphically.

The influences of nanoparticles' shapes on the heat transfer rate based on the average Nusselt number for two different tilt angles and Rayleigh numbers are presented in Figure 6. Effect of nanoparticle shape on the heat transfer rate is not negligible, although it is not as

Table III. Comparison of present results with the Bejan number of published works by Oliveski *et al.* (2009) and Khorasanizadeh *et al.* (2013)

	$Ra = 10^3$		$Ra = 10^4$	
Authors	$\Phi = 10^{-2}$	$\Phi = 10^{-4}$	$\Phi = 10^{-2}$	$\Phi = 10^{-4}$
Present results	0.246	0.967	0.0024	0.189
Oliveski *et al.* (2009)	0.250	0.96	0.0023	0.183
Khorasanizadeh *et al.* (2013)	0.256	0.9701	0.0024	0.19

Table IV. Comparison of average nusselt number along curved cold walls for two different cases, Rayleigh numbers and one specific solid volume fraction ($\varphi = 0.02$ per cent)

	$\theta = 0°$		$\theta = 90°$	
Average nusselt no.	$Ra = 10^3$	$Ra = 10^5$	$Ra = 10^3$	$Ra = 10^5$
Nu_{avg}				
51 × 151	1.981	2.618	1.462	1.952
61 × 181	1.993	2.866	1.688	2.001
71 × 211	2.180	2.905	1.693	2.158
81 × 241	2.237	2.914	1.710	2.213
91 × 271	2.244	2.917	1.716	2.230
101 × 301	2.245	2.917	1.718	2.231

		$\theta = 0°$		$\theta = 90°$	
		$Ra = 10^3$	$Ra = 10^5$	$Ra = 10^3$	$Ra = 10^5$
Platelet		2.244	2.917	1.716	2.230
Cylinder		2.198	2.901	1.711	2.227
Brick		2.183	2.886	1.707	2.219
Spherical		2.180	2.880	1.695	2.208

Figure 6. Effect of shape factor on the magnitudes of average Nusselt number at $\varphi = 0.02$ per cent

significant as the influence of other governing parameters such as Rayleigh number. It is note that any slight influences on the heat transfer rate will change the design process of a heat exchanger and its thermal performance. In this context, the influences of nanoparticles' shapes on the heat transfer rate are compared at two different tilt angles and Rayleigh numbers based on the average Nusselt number. It can be seen that the platelet nanoparticles render higher magnitude of average Nusselt number. Overall, the order of average Nusselt number based on the shapes of nanoparticles is as Platelet > Cylinder > Brick > Spherical. The platelet nanoparticles are selected to be used for further investigations.

The isotherms at different Rayleigh numbers ($10^3 > Ra > 10^6$) and thermal arrangements ($\theta = 0°$, $\theta = 45°$ and $\theta = 90°$) and one specific solid volume fraction of nanofluid ($\varphi = 0.02$ per cent) are presented in Figure 7. The main parameters, which have remarkable impact on the isothermal maps, are the Rayleigh number and tilt angles. With increasing of the Rayleigh number, the patterns of isotherms become disordered. It is due to stronger nanofluid flow, as Rayleigh number enhances, which is able to transfer heat energy in the fluid media. It should be noted that the disordered flow has positive effect on the heat transfer rate because of more collisions of particles.

The streamlines at different Rayleigh numbers ($10^3 > Ra > 10^6$) and thermal arrangements ($\theta = 0°$, $\theta = 45°$ and $\theta = 90°$) and one specific solid volume fraction of nanofluid ($\varphi = 0.02$ per cent) are presented in Figure 8. As Rayleigh number increases, the strength of nanofluid flow enhances. This matter can be concluded by the compacted streamlines at higher Rayleigh numbers. It can be observed that the streamlines are more compacted at the adjacent of active bodies. It is due to the fact that the velocity of nanofluid stream enhances as the density of nanofluid stream reduces due to enhancing the local temperature magnitude at the adjacent of hot walls. It can be occurred near the cold walls by descending stream as a result of density augmentation. On the other hand, the tilt angle causes changing the flow pattern as the direction of nanofluid stream changes as the direction of buoyancy force changes.

The heat transfer irreversibility maps at different Rayleigh numbers ($10^3 > Ra > 10^6$) and thermal arrangements ($\theta = 0°$, $\theta = 45°$ and $\theta = 90°$) and one specific solid volume

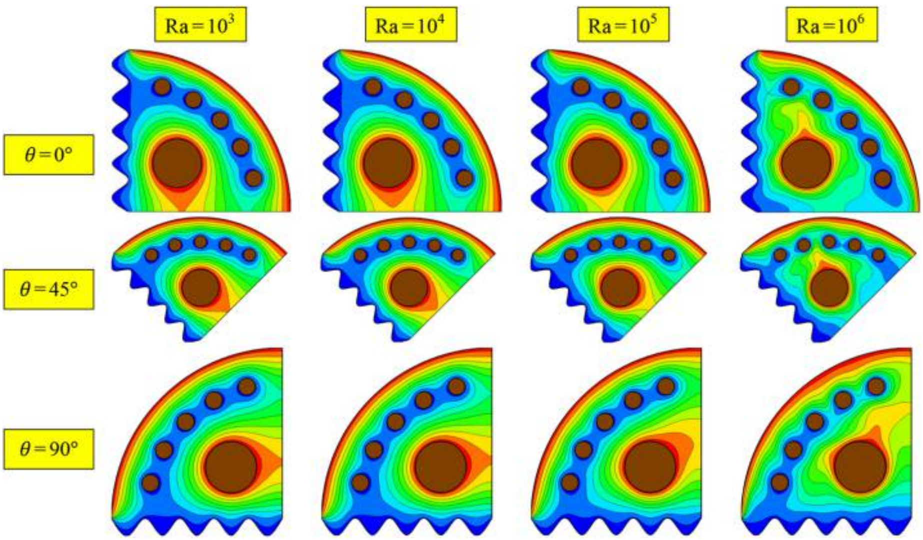

Figure 7.
Temperature fields at different Rayleigh numbers, tilt angles and one specific nanoparticle concentration of φ = 0.02 per cent

fraction of nanofluid (φ = 0.02 per cent) are presented in Figure 9. The main reason of heat transfer irreversibility is the temperature difference between two points in the fluid media. In this context, it can be concluded that the higher magnitude of temperature difference causes higher heat transfer irreversibility. As it can be observed, the heat transfer irreversibility is mainly constituted at the adjacent of active walls such as internal bodies. On the other hand, the constituting of heat transfer irreversibility has direct relationship with the magnitude of Rayleigh number.

The fluid friction irreversibility maps at different Rayleigh numbers ($10^3 > \mathrm{Ra} > 10^6$) and thermal arrangements ($\theta = 0°$, $\theta = 45°$ and $\theta = 90°$) and one specific solid volume fraction of nanofluid (φ = 0.02 per cent) are presented in Figure 10. The fluid friction irreversibility is one of the constituting parameter of total entropy generation. The velocity gradient between two layers of fluid causes fluid friction irreversibility. As such, it is expected that the magnitude of fluid friction irreversibility be dominant at the regions where the fluid stream accelerates. In this context, it can be seen that this parameter has heist magnitude at the adjacent of vertical active walls. On the other hand, the increasing of Rayleigh number causes enhancing the fluid friction irreversibility.

The magnitudes of average Nusselt number at different Rayleigh numbers, nanoparticle concentrations and tilt angles are presented in Figure 11. The magnitude of average Nusselt

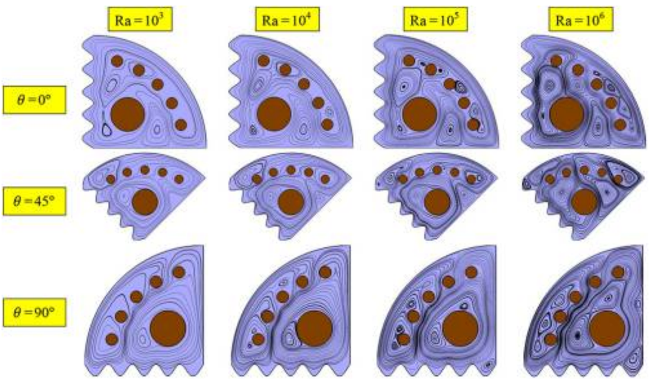

Figure 8. Streamlines at different Rayleigh numbers, tilt angles and one specific nanoparticle concentration of φ = 0.02 per cent

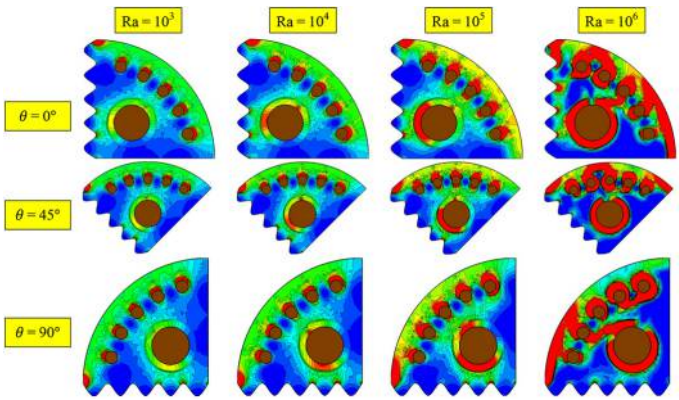

Figure 9. Heat transfer irreversibility maps at different Rayleigh numbers, tilt angles and one specific nanoparticle concentration of φ = 0.02 per cent

number enhances with increasing of Rayleigh number as the pattern of nanofluid stream becomes wavy, and the convective heat transfer will have main effect on the heat transfer rate. On the other hand, adding nanoparticles to the pure water has positive influence on the heat transfer rate due to improved thermal conductivity. Impact of tilt angle on the average Nusselt number is not negligible. The order of the magnitude of average Nusselt number based on the tilt angle is as $\theta = 0° > \theta = 45° > \theta = 90°$.

The magnitudes of total entropy generation at different Rayleigh numbers, nanoparticle concentrations and tilt angles are presented in Figure 12. The magnitude of total entropy generation is based on the fluid friction irreversibility and heat transfer irreversibility and depends on many governing parameters such as Rayleigh number, operating fluid and

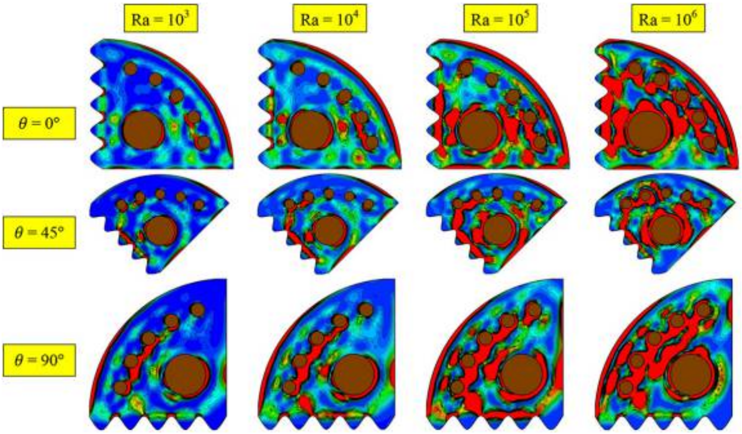

Figure 10. Fluid friction irreversibility maps at different Rayleigh numbers, tilt angles and one specific nanoparticle concentration of φ = 0.02 per cent

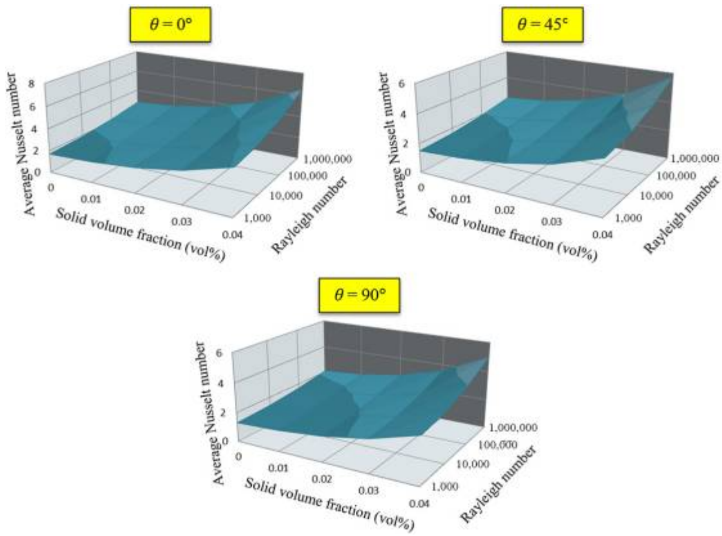

Figure 11. Average Nusselt numbers at different Rayleigh numbers and nanoparticle concentrations

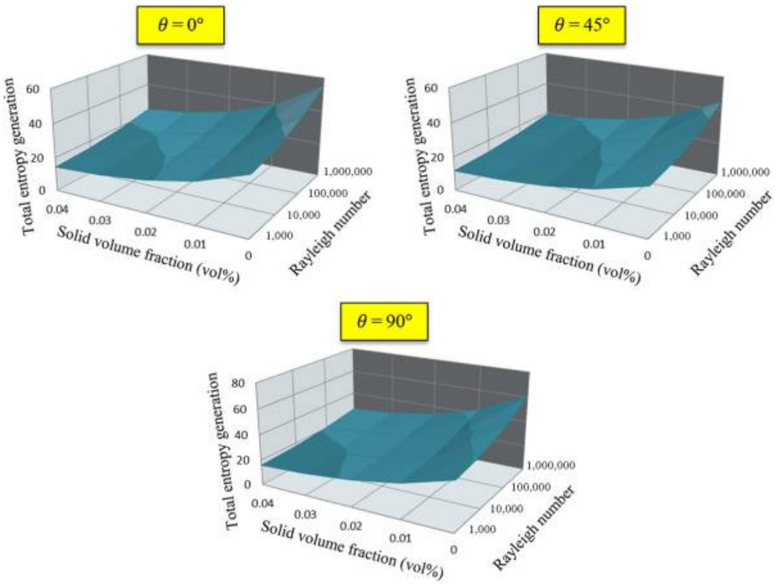

Figure 12.
Magnitudes of total entropy generation at different Rayleigh numbers and nanoparticle concentrations

physical/thermal boundary conditions. As it can be seen, the Rayleigh number has positive effect on the total entropy generation. Moreover, the magnitude of total entropy generation reduces with adding nanoparticles as the temperature field becomes uniform and the strength of nanofluid stream decreases. The order of total entropy generation based on the tilt angles is as $\theta = 90° > \theta = 0° > \theta = 45°$.

The magnitudes of Bejan number at different Rayleigh numbers, nanoparticle concentrations and tilt angles are presented in Figure 13. The Bejan number is a dimensionless parameter which will be used in the entropy generation analysis. The Bejan number shows the share of fluid friction irreversibility and heat transfer irreversibility in the total entropy generation. The Bejan number has direct relationship with the Rayleigh number and nanoparticle concentration. On the other hand, the rule of thermal arrangements of internal pipes is not negligible. The order of the magnitude of the Bejan number based on the tilt angle is as $\theta = 45° > \theta = 0° > \theta = 90°$.

6. Conclusion

The nanofluid flow and heat transfer during natural convection phenomenon are analysed, comprehensively. The entropy generation based on local and total approach is used. For performing numerical simulations, the finite volume method is used, and the KKL model is used to consider the Brownian motion. The CuO-water nanofluid is used as operating fluid. Furthermore, the shapes of nanoparticles are taken account in the analysis. The Rayleigh number, nanoparticle concentration and thermal arrangements of internal active bodies are the governing parameters. It is concluded that the nanoparticles' shapes have minor effect on the heat transfer rate with respect to other parameters. Moreover, Adding nanoparticles to the pure fluid increases and reduces average Nusselt number and entropy generation, respectively. The average Nusselt number and total entropy generation have direct relationship with the Rayleigh number. On the contrary, the total entropy generation has reverse relationship with the solid volume fraction of nanofluid. On the other hand, the

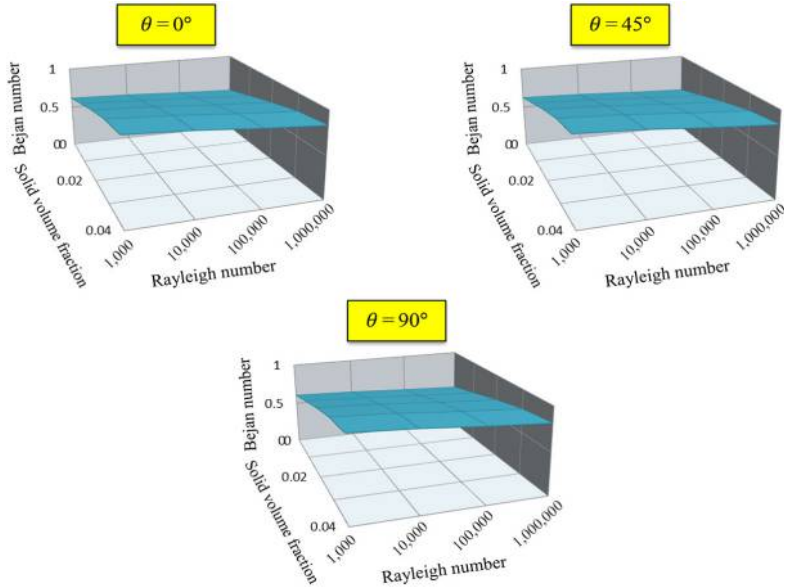

Figure 13.
Magnitudes of Bejan number at different Rayleigh numbers and nanoparticle concentrations

Bejan number has direct and reverse relationship with the solid volume fraction and Rayleigh number, respectively.

References

Bejan, A. (2013), *Convection Heat Transfer*, John Wiley and Sons.

Ben-Nakhi, A. and Chamkha, A.J. (2006a), "Natural convection in inclined partitioned enclosures", *Heat and Mass Transfer*, Vol. 42 No. 4, pp. 311-321.

Ben-Nakhi, A. and Chamkha, A.J. (2006b), "Effect of length and inclination of a thin fin on natural convection in a square enclosure", *Numerical Heat Transfer*, Vol. 50 No. 4, pp. 381-399.

Ben-Nakhi, A. and Chamkha, A.J. (2007a), "Conjugate natural convection around a finned pipe in a square enclosure with internal heat generation", *International Journal of Heat and Mass Transfer*, Vol. 50 Nos 11/12, pp. 2260-2271.

Ben-Nakhi, A. and Chamkha, A.J. (2007b), "Conjugate natural convection in a square enclosure with inclined thin fin of arbitrary length", *International Journal of Thermal Sciences*, Vol. 46 No. 5, pp. 467-478.

Bianchi, A.-M., Fautrelle, Y. and Etay, J. (2004), *Transferts Thermiques: PPUR Presses Polytechniques*.

Ferziger, J.H. and Peric, M. (2012), *Computational Methods for Fluid Dynamics*, Springer Science and Business Media.

Fontes, D.H., Padilla, E.L.M., dos Santos, D.D.O. and Bandarra Filho, E.P. (2017), "Numerical study of the natural convection of nanofluids based on mineral oil with properties evaluated experimentally", *International Communications in Heat and Mass Transfer*, Vol. 85, pp. 107-113.

Kandelousi, M.S. (2014), "KKL correlation for simulation of nanofluid flow and heat transfer in a permeable channel", *Physics Letters A*, Vol. 378, pp. 3331-3339.

Khorasanizadeh, H., Nikfar, M. and Amani, J. (2013), "Entropy generation of Cu–water nanofluid mixed convection in a cavity", *European Journal of Mechanics-B/Fluids*, Vol. 37, pp. 143-152.

Koca, A., Oztop, H.F. and Varol, Y. (2007), "The effects of prandtl number on natural convection in triangular enclosures with localized heating from below", *International Communications in Heat and Mass Transfer*, Vol. 34 No. 4, pp. 511-519.

Lewis, R.W., Morgan, K., Thomas, H. and Seetharamu, K. *The Finite Element Method in Heat Transfer Analysis*, John Wiley and Sons. (1996).

Mahmoud, S., Mehdi, R.M., Emad, H.M. and Masoud, H.M. (2017), "Numerical analysis of turbulent/transitional natural convection in trapezoidal enclosures", *International Journal of Numerical Methods for Heat and Fluid Flow*, Vol. 27, pp. 2902-2923.

Malekshah, M.H., Malekshah, E.H., Salari, M., Rahimi, A., Rahjoo, M. and Kasaeipoor, A. (2018), "Thermal analysis of a cell of lead-acid battery subjected by non-uniform heat flux during natural convection", *Thermal Science and Engineering Progress*, Vol. 5, pp. 317-326.

Oliveski, R.D.C., Macagnan, M.H. and Copetti, J.B. (2009), "Entropy generation and natural convection in rectangular cavities", *Applied Thermal Engineering*, Vol. 29 Nos 8/9, pp. 1417-1425.

Oztop, H.F. and Abu-Nada, E. (2008), "Numerical study of natural convection in partially heated rectangular enclosures filled with nanofluids", *International Journal of Heat and Fluid Flow*, Vol. 29 No. 5, pp. 1326-1336.

Patankar, S.V. (1980), "Numerical heat transfer and fluid flow: computational methods in mechanics and thermal science".

Purusothaman, A. (2018), "Investigation of natural convection heat transfer performance of the QFN-PCB electronic module by using nanofluid for power electronics cooling applications", *Advanced Powder Technology*, Vol. 29 No. 4, pp. 996-1004.

Purusothaman, A., Baïri, A. and Nithyadevi, N. (2016a), "3D natural convection on a horizontal and vertical thermally active plate in a closed cubical cavity", *International Journal of Numerical Methods for Heat and Fluid Flow*, Vol. 26, pp. 2528-2542.

Purusothaman, A., Divya, V., Nithyadevi, N. and Oztop, H. (2016b), "An analysis on free convection cooling of a 3×3 heater array in rectangular enclosure using Cu-EG-Water nanofluid", *Journal of Applied Fluid Mechanics*, Vol. 9.

Purusothaman, A., Oztop, H., Nithyadevi, N. and Abu-Hamdeh, N.H. (2016c), "3D natural convection in a cubical cavity with a thermally active heater under the presence of an external magnetic field", *Computers and Fluids*, Vol. 128, pp. 30-40.

Purusothaman, A., Nithyadevi, N., Oztop, H., Divya, V. and Al-Salem, K. (2016d), "Three dimensional numerical analysis of natural convection cooling with an array of discrete heaters embedded in nanofluid filled enclosure", *Advanced Powder Technology*, Vol. 27 No. 1, pp. 268-280.

Rahimi, A., Kasaeipoor, A. and Malekshah, E.H. (2018a), "Natural convection and entropy generation analysis for 3D inclined enclosure filled with stratified fluids of Ag-MgO/Water hybrid nanofluid and air", *Heat Transfer Research*.

Rahimi, A., Kasaeipoor, A., Malekshah, E.H. and Amiri, A. (2018b), "Natural convection analysis employing entropy generation and heatline visualization in a hollow L-shaped cavity filled with nanofluid using lattice Boltzmann method- experimental thermo-physical properties", *Physica E: Low-Dimensional Systems and Nanostructures*, Vol. 97, pp. 82-97.

Rahimi, A., Kasaeipoor, A., Malekshah, E.H., Far, A.S. and Sepehr, M. (2018c), "Heat transfer intensification using CuO-water nanofluid in a finned capsule-shaped heat exchanger using lattice Boltzmann method", *Chemical Engineering and Processing – Process Intensification*, Vol. 127, pp. 17-27.

Rahimi, A., Kasaeipoor, A., Amiri, A., Doranehgard, M.H., Malekshah, E.H. and Kolsi, L. (2018d), "Lattice Boltzmann method based on Dual-MRT model for three-dimensional natural convection and entropy generation in CuO–water nanofluid filled cuboid enclosure included with discrete active walls", *Computers and Mathematics with Applications*, Vol. 75, pp. 1795-1813.

Rahimi, A., Rahjoo, M., Hashemi, S.S., Sarlak, M.R., Malekshah, M.H. and Malekshah, E.H. (2018e), "Combination of dual-MRT lattice boltzmann method with experimental observations during free convection in enclosure filled with MWCNT-MgO/Water hybrid nanofluid", *Thermal Science and Engineering Progress*, Vol. 5, pp. 422-436.

Rahimi, A., Sepehr, M., Lariche, M.J., Kasaeipoor, A., Malekshah, E.H. and Kolsi, L. (2018f), "Entropy generation analysis and heatline visualization of free convection in nanofluid (KKL model-based)-filled cavity including internal active fins using lattice Boltzmann method", *Computers and Mathematics with Applications*, Vol. 75, pp. 1814-1830.

Salari, M., Kasaeipoor, A. and Malekshah, E.H. (2018a), "Influence of static bubbles at the surface of electrodes on the natural convection flow for application in high performance lead-acid battery", *Thermal Science and Engineering Progress*, Vol. 5, pp. 204-212.

Salari, M., Kasaeipoor, A. and Malekshah, E.H. (2018b), "Three-dimensional natural convection and entropy generation in tall rectangular enclosures filled with stratified nanofluid/air fluids", Vol. 49, pp. 685-702.

Salari, M., Malekshah, E.H. and Esfe, M.H. (2017a), "Three dimensional simulation of natural convection and entropy generation in an air and MWCNT/water nanofluid filled cuboid as two immiscible fluids with emphasis on the nanofluid height ratio's effects", *Journal of Molecular Liquids*, Vol. 227, pp. 223-233.

Salari, M., Hasani Malekshah, E., Hasani Malekshah, M., Alavi, M. and Hajihashemi, R. (2017b), "3D numerical analysis of natural convection and entropy generation within tilted rectangular enclosures filled with stratified fluids of MWCNTs/water nanofluid and air", *Journal of the Taiwan Institute of Chemical Engineers*, Vol. 80, pp. 624-638.

Sheikhzadeh, G., Arefmanesh, A., Kheirkhah, M. and Abdollahi, R. (2011), "Natural convection of Cu–water nanofluid in a cavity with partially active side walls", *European Journal of Mechanics-B/Fluids*, Vol. 30 No. 2, pp. 166-176.

Suárez, M.J., Sanjuan, C., Gutiérrez, A.J., Pistono, J. and Blanco, E. (2012), "Energy evaluation of an horizontal open joint ventilated façade", *Applied Thermal Engineering*, Vol. 37, pp. 302-313.

Verhoeven, J. (1969), "Experimental study of thermal convection in a vertical cylinder of mercury heated from below", *Physics of Fluids*, Vol. 12 No. 9, pp. 1733-1740.

Corresponding author
Emad Hasani Malekshah can be contacted at: emadhasani1993@gmail.com